

DD

E14-95-97

CERN LIBRARIES, GENEVA




SCAN-9509039

su 3536

RADIATION HARDNESS OF SILICON DETECTORS
FOR COLLIDER EXPERIMENTS

Submitted to «Nuclear Instruments and Methods»


1995



Макет Т.Е.Попеко

Подписано в печать 19.05.95
Формат 60×90/16. Офсетная печать. Уч.-изд.листов 3,12
Тираж 340. Заказ 48208. Цена 1872 р.

Издательский отдел Объединенного института ядерных исследований
Дубна Московской области



1. INTRODUCTION

As it has been mentioned in LOI of the L3P and CMS experiments at the LHC a large scale application of silicon pad detectors is supposed for calorimetry. The ENDCAP electromagnetic calorimeter for the L3P experiment contains silicon pad detectors with active area of 690 m^2 .^{/1,2/} For the ENDCAP hadron calorimeter at the CMS experiment the active area of silicon pad detectors is 400 m^2 .^{/3/}

There is another application of silicon detectors - inner tracking systems. Strip Si-detectors with a pitch of 200 microns are considered an alternative to microstrip gas chambers for the inner tracking system in high energy physics experiments. The total area should be not less than several hundred meters of such detectors. Basing on the Dubna Silicon Program the following activity is carried out: detector topology and technology elaboration and research of the detector radiation hardness. This program also includes R&D in the following directions:

- pad detectors for calorimetry;
- photodetectors for the ENDCAP electromagnetic calorimeter;
- strip detectors with a pitch more than 200 microns for inner tracking systems and preshowers.

Guidelines of this program are formulated in the P34 R&D proposal (the Dubna Silicon Program).^{/4/}

For the integrated luminosity of 10^{42} cm^{-2} corresponding to 10 years of LHC running the application of silicon pad detectors used as an active media in the calorimetry requires to study the radiation hardness up to fluences of $6.0 \cdot 10^{13} \text{ cm}^{-2}$. The main consequences for silicon pads exposed in the fast neutron irradiation fields are:

- radiation damage of a silicon bulk resulting in generation of damaged regions and point defects with deep levels in the forbidden gap;
- decrease of the carrier lifetime;
- leakage current increase due to the bulk generation of

carriers which is characterized by the coefficient of $4.0 \cdot 10^{-17}$ A/cm;

- change of the effective impurity concentration and inversion of the conductivity type of the detector bulk (the primary n-type conductivity is inverted into the p-type conductivity due to the donor removal and acceptor-like behavior of the defects created by fast neutrons);
- change of the full depletion voltage during irradiation and, hence, the operative voltage applied to the detector;
- decrease of the charge collection efficiency^{/5/} and increase of the reverse bias voltage for the full charge collection of non-equilibrium charge carriers created by the minimum ionizing particles (m.i.p.).

The aim of the investigation was formulated as follows:

- measurements of electrical parameters of the detectors under fast neutron irradiation;
- silicon bulk degradation research using different methods to develop the detector topology and technology.

The experimental results are accompanied by physical comments on the observed effects and methods of the investigation.

2. SILICON DETECTORS AND INVESTIGATION METHODS

Since 1990 using "Dubna Silicon Program" the radiation hardness study of Si-detectors has been carried out on the fast neutron beam with the average energy of 1MeV at the JINR Fast Pulsed Reactor. Detectors were manufactured of the Float-Zone high resistivity silicon supplied by two companies (WACKER, initial resistivity of 4-10 kOhm*cm and ZTMF, Zaporozhie Titanium Magnezium Factory, Ukraine, 1-4 kOhm*cm).

Fig.1 presents the design lay-out of the experimental silicon pad detectors developed and produced in Russia (ELMA, Zelenograd) and Dubna.

The main purpose of the Si-detector topology and technology development is to produce detectors with parameters adequate to the experiment requirements and still preserving the low cost of detectors at the same time. The cost of silicon pad detectors is 2 CHF/cm² if 500 m² are required and it reduces to 1.2 CHF/cm² - if 2000 m² including the price of the raw material.

Fig.2 shows the reverse current (I_{rev}) distribution for detectors at the bias voltage U of 20% more than the full depletion voltage (U_{FD}).

To determine the initial lifetime τ_r of the minority carriers and its alteration after irradiation we have used the carrier injection- extraction method. Deep levels in the silicon bulk caused by neutron irradiation defects, such as vacancy-oxygen (V-O), vacancy-phosphorus and divacancies in a single- and double- minus charged state (VV^- , $VV^=$) have been measured with the Deep Level Transient Spectroscopy (DLTS). The Shockley-Read-Hall model has been used to determine a contribution of neutron irradiation defects to the increase of the detector reverse current. The redistribution of the electric field in the detectors and, accordingly, the kinetics of the charge carrier transportation have been investigated with the Transient Current Technique (TCT).^{6'} Changes of the charge collection efficiency have been studied with the precise α -particle spectroscopy.^{7'} The conductivity type inversion phenomenon has been confirmed by the following:

- temperature dependence of the Hall constant measured upon special satellite samples;
- electrical (C-V) measurements;
- analysis of the current pulse response to the pulse generation of charge carriers near the front and back sides of the detector.

Table 1 represents the summarized data upon the full set of silicon detectors used in the irradiation research.

3. IRRADIATION FACILITIES

Neutron irradiation of samples has been carried out at JINR facilities using the Fast Pulsed Reactor.^{8/} Pulse duration was $245\mu\text{s}$ at FWHM with frequency of 5 Hz. The energy spectrum is shown in Fig.3. Resonant and epithermal neutrons and γ -rays are absorbed by the filter consisting of Pb - 2 cm thick and B_4C - 1 cm thick, while fast neutrons at the energy $E_n > 0.5$ MeV are not absorbed. For this energy range the flux uniformity of better than 3+5% is kept in the area of $10 \times 10 \text{ cm}^2$ and that is acceptable for detector exposing.

The fast neutron flux equal to $3 \times 10^8 \text{ n/cm}^2 \cdot \text{s}$ is controlled with the standard activation method of intensity measurements using γ -decay of ^{58}Co arisen from $^{58}\text{Ni}(n,p) \rightarrow ^{58}\text{Co}$ nuclear reaction with the energy threshold of 3.45 MeV. At the same time epithermal neutron flux in the energy range $E_n > 10 \text{ eV}$ does not exceed $0.5 \times 10^6 \text{ n/cm}^2 \cdot \text{s}$ depending on energy as $\approx 1/E$. The fast neutron dose absorbed in Al is 0.9 rad/min while γ -ray dose ($E_\gamma \approx 2+2.5 \text{ MeV}$) does not exceed 0.013 Gr/min. The last one is measured by ionizing chambers with Al walls.

The neutron flux and energy spectrum in the exposed area are determined using a set of activation detectors.^{9/} The mean energy of the fast neutron energy spectrum is 1.35 MeV with a summary error of $\leq 20\%$.

4. DEGRADATION OF SI BULK PROPERTIES UNDER NEUTRON IRRADIATION

Degradation of Si detector characteristics under irradiation is determined by changes in electrical parameters of a starting semiconductor as well as the Si-SiO₂ interface. The generation of radiation defects in the crystal lattice leads to the decrease of the minority carrier lifetime and generation lifetime which is followed by the reverse current growth and increase of the charge carrier loss. The other aspect of the defect generation consists in non-monotonous alteration of the effective impurity concentration N_{eff} and

adequate change of the full depletion voltage. Hence, the investigation of the defect formation is essential.

The peculiarity of the damage induced by fast neutrons is connected with the primary defects (vacancies and interstitials) accumulated within the local damaged regions. The defects generated in the periphery of the regions can escape and join the impurities. The interstitials, as the most mobile defects, can escape from the center of the regions whereas vacancies interact with some defects or elements. Thus, under neutron irradiation the defect formation results in both: the generation of point defects and defect accumulation in the damaged regions (clusters). Clusters reduce the potential relief fluctuations in the crystal lattice.^{10,11/} Formation of the potential relief causes changes of electrical properties different from those induced by charged particles or γ -rays.

To investigate bulk degradation the Hall effect and DLTS measurements have been carried out. The DLTS method is widely used to study the point defects with deep energy levels in the forbidden gap^{12-16/} and estimate changes in the generation rate of charge carriers. The Hall effect measurements provide additional information about the deep level generation in the Si bulk.

It should be stressed that the data obtained with these two methods differ because of the details in the measurement procedure and sample manufacturing. The Hall effect measurements have been carried out on special satellite samples made of the bulk material. In this case the measurement mode requires a low bias voltage and practically meets quasi-equilibrium conditions of the neutral bulk. As for the DLTS method, the measurement procedure implies the charge carrier emission into the space charge region of the p-n junction under alternating bias voltage that is far from the steady-state conditions. Besides, to manufacture the p-n junction in the Si detector includes thermal treatment of the initial semiconductor. This introduces thermal defects and

changes the impurity and defect distribution. Hence, the Hall effect data should be considered a direct characteristic of the bulk material rather than the DLTS data. Thus, in addition to the numerous DLTS data available for neutron irradiated detectors, the application of the Hall effect measurements to investigate the degradation phenomena developed in the present work seems to be interesting.

The dependence of free electron concentration n on reciprocal temperature $1/T$ has shown that the initial samples (from Wacker Si) contained not only phosphorus (10^{12} cm^{-3}) slightly compensated by acceptors (presumably boron, $4 \times 10^{10} \text{ cm}^{-3}$) but also some deep donor, $E_c - 0.24 \text{ eV}$, at concentration of about $5 \times 10^{11} \text{ cm}^{-3}$ (Fig.4, curve 1). At the smallest observed fluence $\Phi = 2.0 \times 10^{11} \text{ cm}^{-2}$ the phosphorus concentration diminishes by the value of $2.5 \times 10^{11} \text{ cm}^{-3}$ while concentration of compensating acceptors increases by the same value (Fig.4, curve 2). A possible explanation is in the partial conversion of phosphorus into deep acceptor - E-center (V-P) by means of capturing vacancies escaped from the local neutron damaged regions.

At the fluence of $3.3 \times 10^{12} \text{ cm}^{-2}$ one could expect phosphorus to be almost completely converted into the E-center. Indeed, the temperature dependence of electron concentration (Fig.4, curve 3) reveals the deep level $E_c - 0.45 \text{ eV}$ close to the conventional position of the E-center. The initial deep donors become partially compensated with the E-centers induced by radiation (deep acceptors at concentration of about 10^{12} cm^{-3}). At the room temperature the Fermi level is much lower than the E-center. Then the E-centers are neutral and the saturated electron concentration should be close to the deep donor concentration of $5 \times 10^{11} \text{ cm}^{-3}$. That is indeed the case up to the fluence of $1.0 \times 10^{13} \text{ cm}^{-2}$.

At the higher fluence of $3.0 \times 10^{13} \text{ cm}^{-2}$ the electron concentration essentially decreases as compared with the previous case which indicates that either initial deep donors

are partly lost or some acceptors are generated at the energy levels below the E-center level. However, the further increase of the fluence up to $5.0 \times 10^{13} \text{ cm}^{-2}$ leads to the increased electron concentration so that the previously observed curve (Fig.4, curve 3) is restored. Thus, the further damage leads either to the generation of donors (at the levels above the E-center level) or disappearance of the acceptors produced earlier.

It should be mentioned that the Hall effect data have shown the n- type conductivity of samples at all the fluences observed. On the other hand, the C-V dependence measured for the irradiated detectors produced from the same silicon ingot, reveals that the overall concentration of the charged centers in the depleted region gradually decreases with fluence. And after the fluence of $8.0 \times 10^{12} \text{ cm}^{-2}$ it starts increasing. After removal of the electrodes we have carried out the Hall effect measurements of such "inverted" detectors and found the n-type conductivity: the Hall curves are quite similar to curve 3 in Fig.4.

This apparent contradiction can be explained as follows. The induced acceptor centers are distributed homogeneously in the bulk and partially clustered in the local damage regions. Due to the high concentration of defects in the clusters the energy bands are bent forming the potential barrier in the vicinity of the cluster.^(10,11) Hence, the local Fermi level may be lower than the acceptor level and it means that the acceptors are only partially charged. In the Hall effect measurements the external voltage is rather low, so, the potential barrier can not be disturbed and the holes are captured within the clusters. Hence, the total charge of the free holes may be lower than the electron charge from the uniformly distributed donors. The sample conductivity will be of n-type despite of the lower donor concentration. As for the C-V and DLTS measurements the external electric field is usually much stronger than the local field of the cluster. And that is why the holes do escape from the cluster leaving

all the cluster acceptors charged.^{17/}

The results discussed above have been obtained for the detectors and samples irradiated at 16°C.

The DLTS measurements have been carried out on detectors twice: just after irradiation and then after the following annealing for 30 days, both at the room temperature. The DLTS spectrum of the defects induced at the fluence of $2.0 \times 10^{11} \text{ cm}^{-2}$ is shown in Fig.5. The parameters of deep levels (activation energy E_a and capture cross-section σ) presented in Table 2 are calculated taking into account the effective impurity concentration determined from the low frequency (0.1-1 kHz) C-V measurements. To identify the defects the isochronal annealing is taken into consideration.

One should note that some energy levels of the defects induced by radiation represent superposition of two complexes with the varying ratio of components. Besides, there are some peculiarities connected with the detector origin.^{12/} Only energy level E2 can be undoubtedly attributed to the double minus charge state of the divacancy (VV^-) while E1 and E3 may contain two defect complexes. Annealing of defect E1 occurs mainly in the temperature range of 180-250°C. We can refer it to the C_1-C_2 complex rather than the A-center (V-O). It was established earlier that energy level E3 represents the sum of two components: the E-center (V-P) and the single minus charge state of the divacancy (VV^-).^{18/} Annealing of E3 occurs in the wide temperature range of 100-250°C without any vivid concentration decrease at 150°C inherent to the E-center annealing. Since the divacancy annealing takes place at $T > 300^\circ\text{C}$, the monotonous decrease of the E3 concentration should be attributed to the divacancy annealing in the local damaged regions with the reduced activation energy of thermal annealing.

It is more difficult to analyze the defects induced by radiation with deep levels in the lower half of the forbidden gap (Fig.5b). The DLTS spectra are affected considerably, first, by the self-annealing process and, next, experimental

requirements, namely, the high injection current density in the filling pulse. It should be noted that methodical aspects of the DLTS measurements on the high resistivity Si compensated by deep levels, are out of the scope of the present paper. In the measurements carried out just after neutron irradiation two main deep levels have been observed: H1 (C_i) and H2 (C_i-O_i). The feature of their behavior in the irradiated Si crystals consists in the carbon-related defect transformation.^{/12,19,20/} In our case the decay of interstitial carbon happens even at the room temperature and it is followed by the concentration increase of the carbon related complexes which include $C_i: C_i-O_i$, C_i-C_i . The analysis of this phenomenon in the detectors irradiated by α -particles has shown that in FZ Si the decay rate is affected essentially by the detector manufacturing procedure.^{/19/}

Another peculiarity of the DLTS spectra consists in appearance of two additional peaks in the lower half of the forbidden gap if to use the high injection current density in the positive filling pulse. Energy level $E_v+0.20$ eV is, probably, connected with the positive charge state of the divacancy (VV) while the origin of energy level $E_v+0.27$ eV ($\sigma=4 \times 10^{-14} \text{ cm}^2$) is not clear yet; the similar peak was observed in the high resistivity Si irradiated by deuterons.^{/20/}

It is very important to analyze the contribution of deep levels into the reverse current of detectors. The generation rate of the center can be evaluated from the carrier generation lifetime τ_{eff} according to the Shockley-Reed-Hall theory:

$$\tau_{eff} = \frac{\sigma_n \exp \frac{E_t - E_i}{kT} + \sigma_p \exp \frac{E_i - E_t}{kT}}{\sigma_p \sigma_n v_{th} N_t} \quad (1)$$

where:

v_{th} - thermal velocity,
 N_t - concentration of deep levels,
 E_i - energy in the middle of the forbidden gap,
 E_t - activation energy of the deep level.

The results of the calculation allow one to arrange the observed deep levels in the decreasing order of their generation activity: $E_3 \rightarrow H_1 \rightarrow H_2 \rightarrow E_1$.^{16/} The total contribution of the deep levels should take into account the defect density, especially for the defects with the largest activation energy.

Additional information on the bulk property degradation has been obtained from the direct measurements of the charge carrier lifetimes. The generation lifetime has been measured on MOS samples from the inversion of the Si conductivity type in the vicinity of the Si-SiO₂ interface and the linear dependence of $(\tau_{gen})^{-1}$ on fluence with damage constant $K_{gen}^{\tau} \approx 2 \times 10^{-8} \text{ cm}^{-2} * \text{s}^{-1 \text{ gen}}$ has been revealed. The carrier injection-extraction method has been used to determine the minority carrier lifetime, the damage constant is $5 \times 10^{-8} \text{ cm}^{-2} * \text{s}^{-1}$.

We suppose that the data on the transformation of the carbon related defects are very important in practice. It can be considered as a possible model of the reverse annealing and long term transformation of the detector characteristics.^{22/}

5. STEADY STATE CHARACTERISTICS OF IRRADIATED DETECTORS

The alteration of the detector characteristics under fast neutron irradiation consists in the following:

- non-monotonous change of the bulk resistivity and effective impurity concentration;
- conductivity type inversion;
- reverse current increase;
- change of the full depletion voltage;
- decrease of the charge collection efficiency.

The aspects of the degradation problem, namely change of I-V and C-V characteristics, the effective impurity

concentration and radiation damage constant have been widely investigated and numerous data are available for different types of detectors.^{23-25/} The aim of our study is to get quantitative information on the pad detectors manufactured by ELMA of two materials with different quality.

The typical set of I-V characteristics of detectors made of Wacker Si and irradiated at different neutron fluences ($2 \cdot 10^{12} \div 6 \cdot 10^{13} \text{ cm}^{-2}$) is presented in Fig.6a. One can compare I-V characteristics of the detectors before and three days after irradiation presented in Fig.7a,b, respectively. Before irradiation the reverse currents of the ZTMF Si detectors exceed those of the Wacker Si detectors with the higher initial resistivity (measurements have been carried out at the same bias voltage for the both types of the detectors). After irradiation at the fluence of $3.0 \cdot 10^{12} \text{ cm}^{-2}$ which is close to the inversion point the reverse current ratio turns into its opposite. As

$$I_{\text{rev}} = \frac{e \eta_1 S W}{\tau_{\text{eff}}} \quad (2)$$

where:

- S - p-n junction area,
- W - thickness of the space charge region,
- τ_{eff} - effective carrier generation lifetime,

one should suppose that for the Wacker Si detectors the increase of W near the inversion point prevails the decrease of τ_{eff} . Hence, the alteration of the reverse current ratio is attributed mainly to the evolution of N_{eff} rather than to the decrease of τ_{eff} .

The reverse current damage coefficient α is determined according to the relation:

$$\Delta I = \alpha V \Phi \quad (3)$$

where $V=SW$ - volume of the space charge region. The dependence of the reverse current per volume on fluence measured two days after irradiation is shown in Fig.8. For the Wacker Si detectors α is $2 \cdot 10^{-17} \text{ A/cm}$ which is in the

range of experimental data for different types of detectors.

Other data which may be used to determine α are presented in Fig.9. At the fixed fluence the product $IC = e\epsilon\epsilon_0 n_1 S^2 / \tau_{eff}$ is a constant independent on voltage. Nevertheless, the experimental value is constant only for the Wacker Si detectors irradiated at large fluences. The relation $IC = \text{const}$ can be considered as the test of the detector quality: its experimental validity would confirm the dominant contribution of the bulk degradation in comparison with other effects.

The C-V characteristics of the Wacker Si detectors irradiated at different fluences and measured at low frequency are shown in Fig.6b. The curves demonstrate the compensation of the semiconductor conductivity resulting in the decrease of N_{eff} and U_{FD} , and their following increase after the inversion. At U_{FD} the detector capacitance is ≈ 100 pF. The full depletion voltage U_{FD} found from C-V characteristics as a function of fluence, is shown in Fig.10.

The results on irradiation of detectors kept under the reverse bias voltage are presented in Fig.11. The difference in the reverse current as a function of fluence for the detectors irradiated with and without the applied bias voltage, is negligible and it is a subject for further investigation.

In conclusion we should emphasize that despite of the numerous and detailed results of C-V measurements on irradiated detectors (including the present work), the non-monotonous evolution of the effective impurity concentration under neutron irradiation with the minimum at the presumed inversion point is not a satisfactory confirmation of the conductivity type inversion. Only the results of the α -particle spectroscopy and TCT measurements would prove the evidence of the electric field redistribution from the p^+ -side to the n^+ -side of the detector confirming the adequate change in the sign of the effective impurity concentration. In a scope of the cluster model the difference

in the effective impurity and free carrier concentrations and their signs may be connected with the filling of deep levels in the forbidden gap and possibility of holes to escape through the potential barrier of the cluster.

6. DEGRADATION OF CHARGE COLLECTION EFFICIENCY UNDER NEUTRON IRRADIATION

In this paragraph the problem of the charge collection efficiency for the detectors before and after neutron irradiation is discussed. For this purpose the charge transport phenomena have been investigated with different experimental methods. Using the α -particle excitation of non-equilibrium carriers the precise measurements of the amplitude deficit as a function of bias voltage have been carried out to determine separately the lifetime of electrons and holes in the space charge region. Using the transient current technique (TCT) the analysis of the current response curves has been made to get information on the signal kinetic and charge collection time. The both methods help to determine the sign of the effective impurity concentration in the space charge region and they confirm the conductivity type inversion at neutron fluences exceeding $8.0 \cdot 10^{12} \text{ cm}^{-2}$. The analysis of the current response to the light pulse excitation enables to interpret the experimental data on the minimum ionizing particle (m.i.p.) excitation.

In general the amplitude deficit ΔA contains three components:

- energy loss ΔA_d in the "dead" layer;
- charge loss ΔA_t due to the carrier trapping as non-equilibrium carriers drift in the space charge region during collection time t_c ;
- kinetic deficit component ΔA_{kin} which depends on the relation between rise-time t_r and amplifier shaping time θ .

$$\Delta A = \Delta A_d + \Delta A_t + \Delta A_{kin} \quad (4)$$

Measurements of the signal amplitude and its deficit have been carried out for the detectors before and after neutron irradiation using the α -particle spectroscopy. The curves of ratio A_p^+/A_n^+ as a function of bias voltage at different neutron fluences are shown in Fig.12, where A_p^+ and A_n^+ are the peak amplitudes for the α -particle incidence on the p^+ -layer and n^+ -layer, respectively; the shaping time is 1 μ s. The amplitudes become equal to each other (within accuracy of about 1×10^{-2}) at the full depletion voltage. Values of $A_p^+/A_n^+ < 1$ indicate that the maximum electric field is located at the back contact. Hence, it concerns the detector with the inverted conductivity type.

Fig.12 presents the amplitude ratio and it can not provide the information on the deficit dealt with the carrier trapping. To analyze the charge collection in details and determine the lifetime of non-equilibrium electrons and holes the precise α -particle spectroscopy with the additional reference detector has been used.⁷⁷ Two α -particle sources with different energies make possible to get the energy scale for the amplitude measurements and exclude any instabilities of the experimental set-up; the achieved accuracy is 10^{-4} . Carried out on the non-irradiated detectors the measurements of the amplitude deficit as a function of reverse bias voltage and the detector tilting angle reveal the deficit to depend mainly on thickness of the detector entrance window. The value of $2.5 \pm 3.0\%$ corresponds to the window thickness of $1.0 \pm 1.2 \mu\text{m}$ including the Al contact film and "dead" layer d_{dead} - the part of the high doped p^+ -layer $\approx 2000 \text{ \AA}$ near the surface (or the n^+ -layer if the back surface is irradiated by α -particles). Determined from the charge collection of non-equilibrium carriers the amplitude deficit equals to 10^{-3} for electrons in the range of reverse bias voltage $U = 50 \pm 200 \text{ V}$ and for holes at $U > U_{\text{FD}}$. The negligible value of the amplitude deficit indicates that there is no trapping for non-equilibrium carriers in the space charge region.

Since the reverse current of irradiated detectors increases up to hundreds μA the measurements of the amplitude deficit have been carried out on the cooled samples ($T = 210 - 230 \text{ K}$). The corresponding temperature shift of the mean amplitude of about 3.4% has been taken into account.

To analyze the lifetime degradation we have used the approximation of the carrier effective lifetime τ_{eff} in the space charge region which is a quantitative characteristic of the charge loss:

$$\Delta A_t = \frac{c^t}{2 \tau_{\text{eff}}} \quad (5)$$

The mode to measure τ_{eff} is $\theta \gg t_r \approx t_c$, that leads to $\Delta A_{\text{kin}} \approx 0$. The equation (5) can be transformed to:

$$\Delta A_t = \frac{1}{2} \frac{d}{\mu \langle E \rangle \tau_{\text{eff}}} \quad (5a)$$

where:

d - detector thickness,

μ - mobility,

$\langle E \rangle$ - mean electric field.

Saturation of the drift velocity is neglected.

Fig. 13 presents the dependences of the amplitude deficit on electric field for electrons and holes (p^+ - and n^+ -layers are bombarded in succession by α -particles of ^{244}Cm) in the irradiated detector before inversion ($\Phi = 3.3 \cdot 10^{12} \text{ cm}^{-2}$). The curve slope gives the values: $\tau_{\text{eff}}^e = 1.1 \mu\text{s}$ and $\tau_{\text{eff}}^h = 0.44 \mu\text{s}$. The lower value of τ_{eff}^h can be attributed to the fact that for the radiation defects with deep levels the capture cross-section for holes is larger compared with that for electrons.^{15/} The carrier lifetimes in the irradiated detector before and after inversion are presented in Table 3. The rapid decrease of τ_{eff}^e as compared with τ_{eff}^h can be explained taking into account the shift of the Fermi level induced by radiation towards the valence band. It leads to

the concentration increase of the centers which can act as effective electron traps.

The average amplitude deficit as a function of shaping time for the both: non- and irradiated detectors, is presented in Table 4. Detectors have been bombarded by α -particles of ^{244}Cm at $U=160$ V. The amplitudes are normalized on the maximum amplitude in the non-irradiated detector. For the non-irradiated detector there is only a slight difference in the charge collection efficiency for electrons and holes (p^+ - and n^+ -layer have been bombarded respectively by α -particles); amplitude deficit variations are less than $2.0 \cdot 10^{-3}$. The small increase of the deficit while q rises from 0.1 ms to 1 ms, becomes detectable due to the high accuracy of the measurements. This effect can be attributed to the changes of the low energy "tail" of the spectra.

Neutron irradiation of detectors leads to the increase of the both: DA^e and DA^h . Hence, the non-equilibrium carrier trapping takes place in irradiated detectors. DA^h has the greater value than DA^e , their difference can grow till 0.06 at the fluence of $1.6 \cdot 10^{13} \text{ cm}^{-2}$. Nevertheless, taking into account the larger drift mobility and velocity of electrons, these values are in agreement with practically equal lifetimes for the electrons and holes measured at this fluence.

DA^e for a fixed neutron fluence has the same dependence on q as for non-irradiated detectors - it has a slight increase by 0.005 while q rises. Meanwhile DA^h decreases by 0.02 when the shaping time increases from 0.1 ms to 1ms. This indicates that the hole detrapping takes place and increases the charge collected in the detector.

7. CHARGE COLLECTION KINETICS

To investigate the fast kinetic processes and measure the kinetic amplitude deficit in the detectors, the transient current technique has been applied.^{6/} Most of the

experimental versions of the method have used α -particles to generate non-equilibrium carriers near the surface (near the p^+ - or n^+ -layer) providing the charge transport study for electrons and holes separately. Application of this TCT version to the detectors irradiated by neutrons enables to connect the shape changes of the current pulse with the inversion of the conductivity type.^{5, 26-28/}

A qualitative consideration of the experimental data on the current response to the α -particle excitation for the both non- and irradiated detectors (Fig.14) has shown that only the hole collection is suitable to estimate accurately the electric field distribution from the shape of the current pulse (curve 2). As for the electron collection (curve 1), the peculiarities connected with the electric field distribution are rather vague. A reasonable explanation is the influence of the carrier trapping and plasma effects inside the high density tracks of α -particles.^{7, 29/} Duration of the plasma stage depends on electric field E and is about 5 ns at $E \approx 4$ kV/cm ($U = 160V$) for α -particles at the energy of 5 MeV.

To eliminate the plasma effect and increase the time resolution of the TCT the excitation by the short laser pulse has been applied. The other advantage of this experimental version is a possibility to make the current pulse observable without a signal preamplification. The GaAs laser has been used to generate the light pulse pumped by the current pulse generator with pulse duration of less than 1 ns. The parameters of the set-up are:

- light pulse duration ≈ 0.7 ns
- effective pulse energy ≤ 100 MeV
- area of the light spot $\geq 400 \times 400 \mu m^2$
- time resolution of the oscilloscope 200 ps

The detailed description of the technique was presented in ^{28/}.

The current response curves for the both: non- and irradiated detectors, are shown in Fig.15. For the partially

depleted detectors the electron component has an exponential decay (Fig.15a) while the hole component (Fig.15b) is very small and has large duration due to the hole diffusion in the neutral base of the detector. When the detector is totally depleted the pulse top is determined by the electric field distribution (Fig.15c,d). The inclination change in the slope of the pulse top for the detector irradiated at the fluence of $3.3 \cdot 10^{13} \text{ cm}^{-2}$ indicates that the inversion under irradiation has taken place. The peculiarity of the irradiated detectors is the "smoothed" shape of the current response curves with large "tails". These "tails" are associated with the fast trapping and detrapping of non-equilibrium carriers.

The duration of the current pulse allows to estimate the kinetic deficit component ΔA_{kin} . Using the RC-shaping with the integral and differential constants equal to θ the kinetic deficit component is:

$$\Delta A_{kin} = 1 - \frac{\theta}{t_r} \left[e^{t_r/\theta} - 1 \right] \exp \left[1 - \frac{t_r}{\theta} \frac{e^{t_r/\theta}}{e^{t_r/\theta} - 1} \right] \quad (6)$$

The data on the calculated ΔA_{kin} are presented in Table 5. We put the rise time equal to the hole collection time $t_r = t_c = 25 \text{ ns}$. The equation (6) can be approximated as $\Delta A_{kin} \approx x^2/24$ at $x \leq 1$ (where $x = t_r/\theta$). At $\theta = 100 \text{ ns}$ $\Delta A_{kin} = 0.26 \cdot 10^{-2}$ that is much lower than the measured one (see Table 4). One should note that at the shaping time of about 20 ns being proposed in the calorimeter projects, ΔA_{kin} does not exceed 0.06 but it increases up to 0.2 at $\theta = 10 \text{ ns}$.

When relativistic particles are detected, the both types of carriers are generated homogeneously along the thickness of the space charge region. It leads to the deficit and collection time increasing in comparison with the case of the surface light pulse or α -particle irradiation. Indeed, for the m.i.p. generation the collection time is about 20 ns for

the both: non- and irradiated detectors, being practically independent on fluence up to the fluence of $4.0 \cdot 10^{13} \text{ cm}^{-2}$ (Fig.16). The value is less than t_c for the holes which have the smaller drift mobility. It should be noted that the increased pulse duration in comparison with $10 \text{ ns}^{5/}$ is connected with the enlarged capacitance of the detector with the area of 4 cm^2 (about 100 pF at the full depletion voltage).

The signal amplitudes equivalent to the charge collection efficiency as a function of neutron fluence at the bias voltages of 100 V and 200 V are presented in Fig.17. The integrating oscilloscope has been used to measure the charge collection efficiency; integration intervals τ_{int} are 10, 20 and 50 ns. At the lower voltage (Fig.17a) the dependences have maximum near the inversion point when the electric field is homogeneous and it leads to the minimal drift time. The deficits measured at $\phi < \phi_i$ exceed the both: calculated kinetic component (Table 5) and experimental one.^{5/}

At the larger fluences the amplitude deficit increases due to the t_r increase and prolonged trapping-detrapping. The sharp decrease of the collected charge occurs at $\phi > 4.0 \cdot 10^{13} \text{ cm}^{-2}$ being especially evident at τ_{int} of 20 and 50 ns. The comparison with the dependence of the full depletion voltage on fluence (Fig.10) has shown that at the fluence of $4.0 \cdot 10^{13} \text{ cm}^{-2}$ and the reverse bias voltage of 100 V, the detector is partially depleted. In this case the current pulse has a slow component attributed to the influence of the induced current in the neutral base region. This region is compensated by the radiation defects with deep levels.^{28/} Maxwell relaxation constant can grow up to $1 \mu\text{s}$ and it increases the deficit in a great extent without any dependence on the integrating constant of tens of ns. At the reverse bias voltage of 200 V (Fig.17b) the detector is kept fully depleted up to the fluence of $4 \cdot 10^{13} \text{ cm}^{-2}$, hence, the amplitude deficit is constant. But it grows if the high compensated neutral base appears at larger fluences.

As for $t_{int} = 10$ ns, the dramatic amplitude decrease at any voltage and fluences lower or near the inversion point, is mainly attributed to the enlarged capacitance of the detector (and the pulse duration, consequently) as compared with other data^{/5,27/} where the area of samples was in the range of $0.25:1.0\text{cm}^2$.

To summarize the experimental data on the charge collection one should note that if the shaping time is larger than 20 ns, the amplitude deficits do not exceed 0.1:0.15 for the totally depleted detectors irradiated at neutron fluences less than $4.0 \cdot 10^{13} \text{ cm}^{-2}$. The trapping-detrapping of non-equilibrium carriers contributes the main share into the amplitude deficit. It has been revealed from the study of the both: amplitude deficit and charge collection kinetics. At larger fluences the detector becomes partially depleted and the amplitude deficit essentially increases. This is attributed to the influence of the high compensated neutral base in which Maxwell relaxation constant can grow up to 1 ms. Hence, for the effective charge collection at larger fluences it is necessary to apply the reverse bias voltage exceeding the full depletion voltage.

In conclusion we would like to express our acknowledgements to F.Lemeilleur (CERN) for his help in measurements.

Table 1

Group of samples	Silicon	Initial:			Technology and topology	Number of samples
		Resistivity, $k\Omega \cdot cm$	Minority carriers lifetime, ms	Effective doping concentration, cm^{-3}		
1 $p^{+}nn^{+}$ PAD detectors	n-type, Wacker-Chemitronic	4...6	≥ 4	$\approx 10^{12}$	n^{+} -implanted, p^{+} -implanted, $20 \times 20 \times 0,4 \text{ mm}^3$	11
2 $p^{+}nn^{+}$ PAD detectors	n-type, Wacker-Chemitronic	4...6	≥ 4	$\leq 10^{12}$	n^{+} -diffused, p^{+} -implanted, $20 \times 20 \times 0,4 \text{ mm}^3$	6
3 $p^{+}nn^{+}$ PAD detectors	n-type, ZTMF, Ukraine	1...2,5	$\sim 0,5$	$(3...5) \cdot 10^{12}$	n^{+} -implanted, p^{+} -implanted, $20 \times 20 \times 0,4 \text{ mm}^3$	7
4 DLTS	n-type, Wacker	4...6	≥ 4	$\leq 10^{12}$	n^{+} -implanted, p^{+} -implanted, $2 \times 2 \times 0,4$ and $5 \times 5 \times 0,4 \text{ mm}^3$	9+9
5 Hall effect measurements	n-type, Wacker	4...6	≥ 4	$\leq 10^{12}$	Initial silicon, $11 \times 3 \times 2 \text{ mm}^3$	11
	n-type, ZTMF	1...2,5	$\sim 0,5$	$(3...5) \cdot 10^{12}$		

Table 2
Parameters of deep levels for radiation induced defects

Level type	Activation energy, eV	Capture cross- section, cm^2
E1	$E_C - 0.18$	$\sigma_n = 2.0 \cdot 10^{-14}$
E2	$E_C - 0.22$	$\sigma_n = 2.0 \cdot 10^{-16}$
E3	$E_C - 0.40$	$\sigma_n = 2.0 \cdot 10^{-16}$
H1	$E_V + 0.33$	$\sigma_n = 9.0 \cdot 10^{-14}$
H2	$E_V + 0.40$	$\sigma_n = 3.0 \cdot 10^{-14}$

Table 3
Effective lifetimes of charge carriers

Fluence	Conductivity type	$\tau_{\text{eff}}^h, \mu\text{s}$	$\tau_{\text{eff}}^e, \mu\text{s}$
$3.3 \cdot 10^{12}$	n	0.44	1.1
$1.6 \cdot 10^{13}$	p	0.11	0.13
$8.0 \cdot 10^{13}$	p	0.055	0.015

Table 4

Average amplitude deficit as a function of shaping time θ

Number of the sample	Fluence, cm^{-2}	Type of drifting carriers	Deficit, arb. units		
			$\theta=0.1\mu\text{s}$	$\theta=0.3\mu\text{s}$	$\theta=1\mu\text{s}$
D5-1	0	e	<0.01	0.17	0.19
		h	<0.01	0.17	0.26
D7-1	$3.3 \cdot 10^{12}$	e	0.81	1.01	1.45
		h	4.52	3.82	2.95
D7-2	$1.6 \cdot 10^{13}$	e	4.73	4.87	5.12
		h	10.82	10.26	8.54

Data are normalized on amplitude of the sample

D5-1 ($\theta = 0.1\mu\text{s}$); e - electrons, h - holes.

Table 5

Calculated kinetic deficit

$\theta, \mu\text{s}$	1.0	0.5	0.25	0.1	0.05	0.02	0.01
ΔA_{kin} , arb. units	$3 \cdot 10^{-5}$	$1.1 \cdot 10^{-4}$	$4 \cdot 10^{-4}$	$2.6 \cdot 10^{-3}$	$1.03 \cdot 10^{-2}$	$6.07 \cdot 10^{-2}$	$2.1 \cdot 10^{-1}$

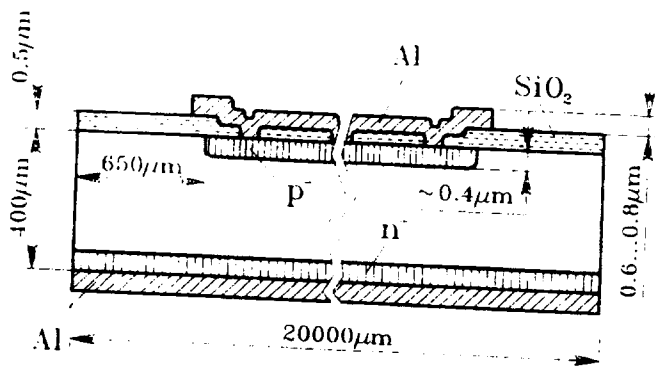


Fig. 1. Detector design lay-out.

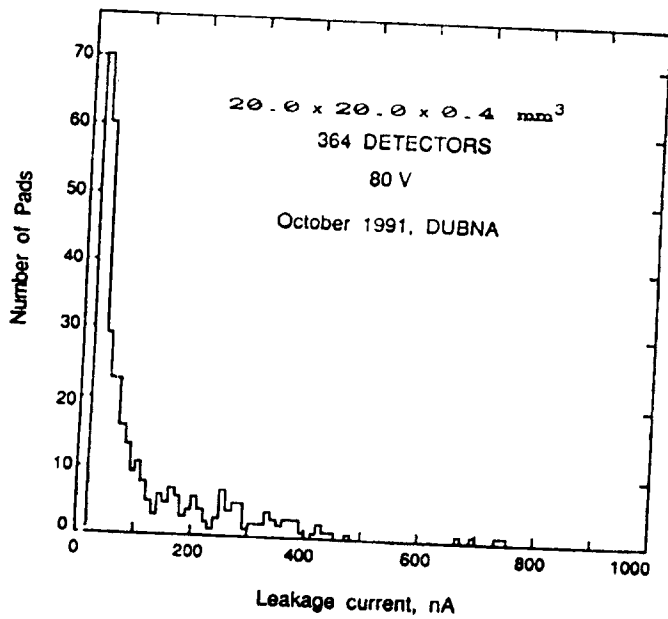


Fig. 2. Distribution of reverse currents for the set of detectors made of Wacker Si. Area: $2 \times 2 \text{ cm}^2$. Bias voltage: 80 V.

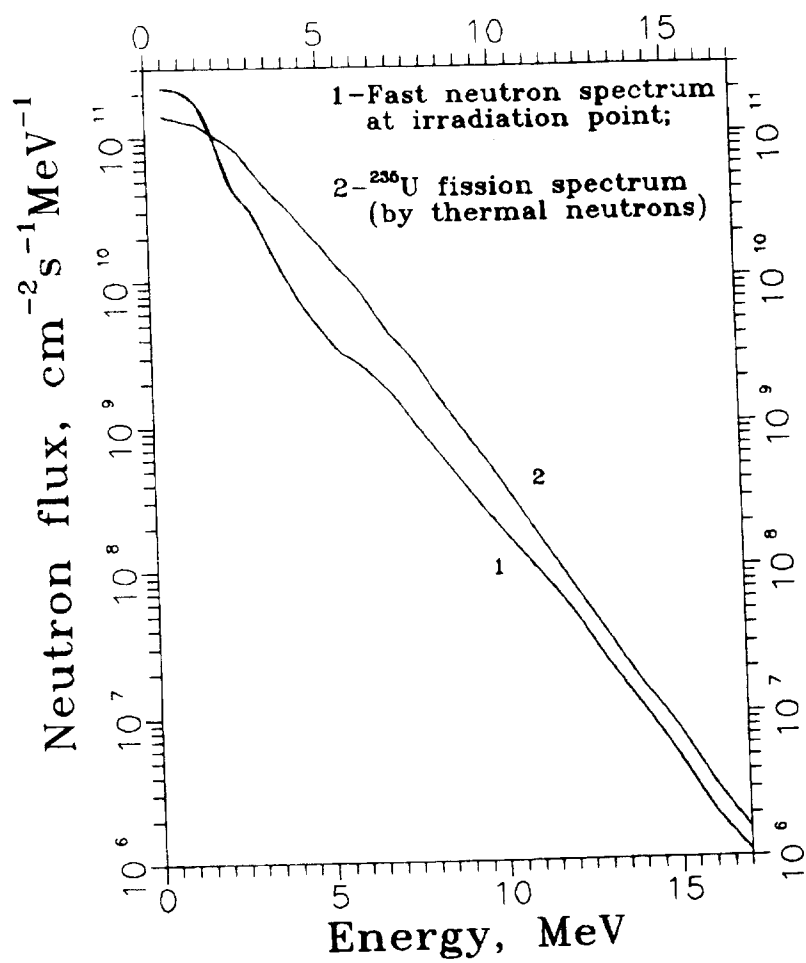


Fig.3. Energy spectrum of neutrons before filtering.

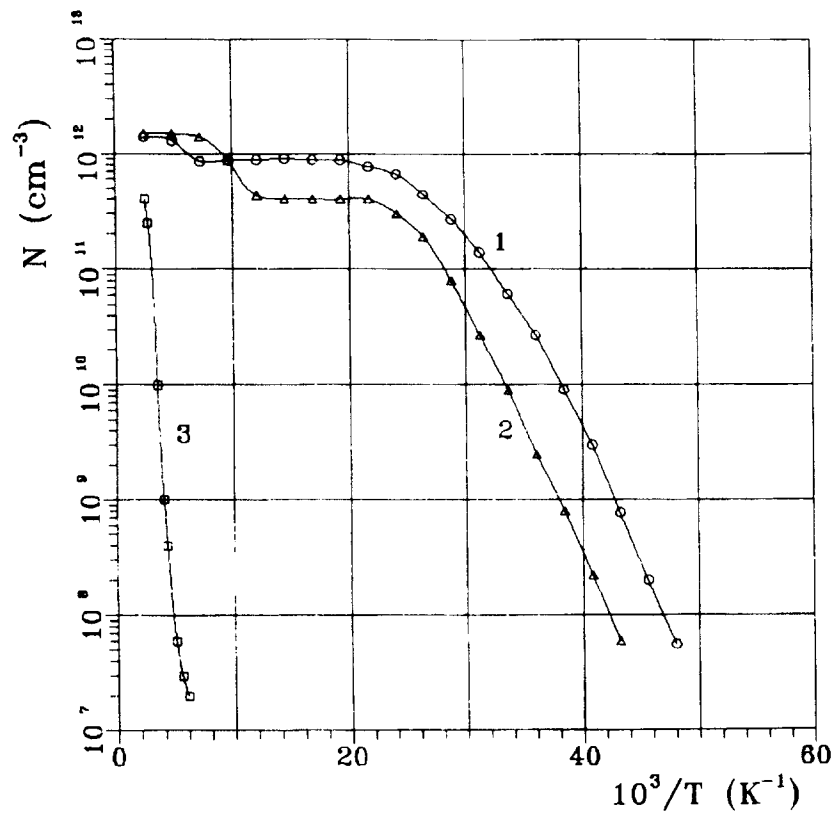


Fig.4. Free electron concentration versus reciprocal temperature: (1) before and (2,3) after neutron irradiation at the temperature of 16°C . Fluence Φ [cm^{-2}]: (2) - $1.0 \cdot 10^{11}$, (3) - $3.3 \cdot 10^{12}$.

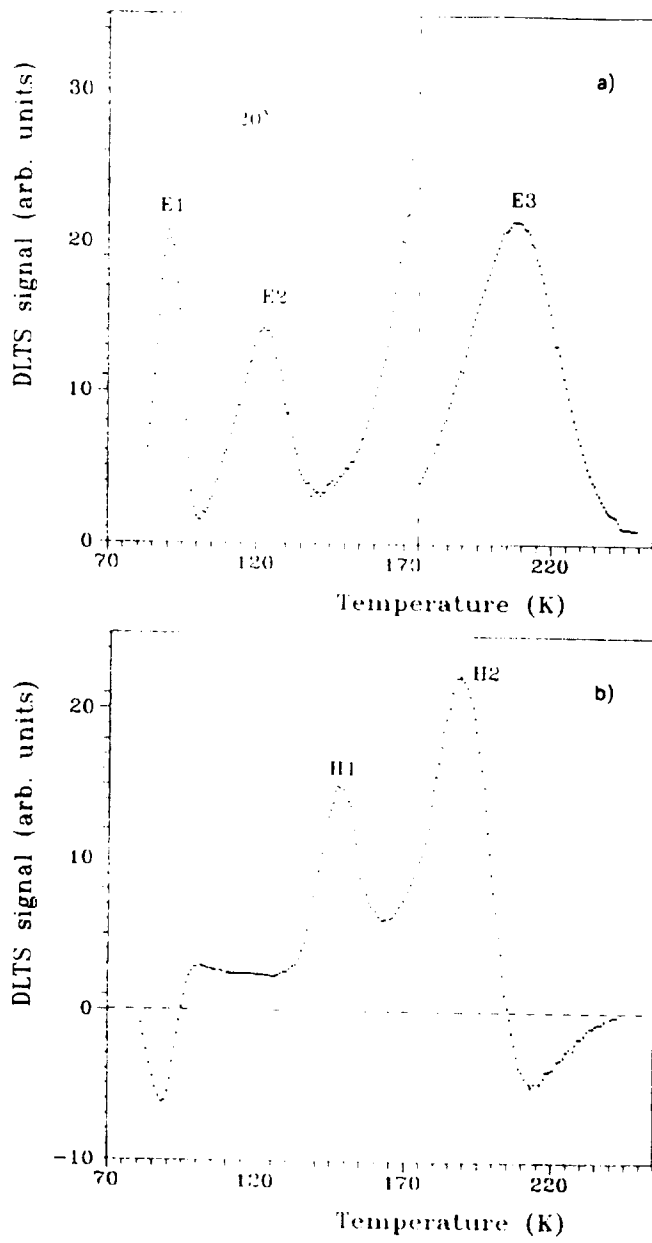


Fig.5. DLTS spectra of deep levels in Si irradiated by neutrons, (a) - in the upper half of the forbidden gap, (b) - in the lower half of the forbidden gap. Fluence: $2 \cdot 10^{11} \text{ cm}^{-2}$.

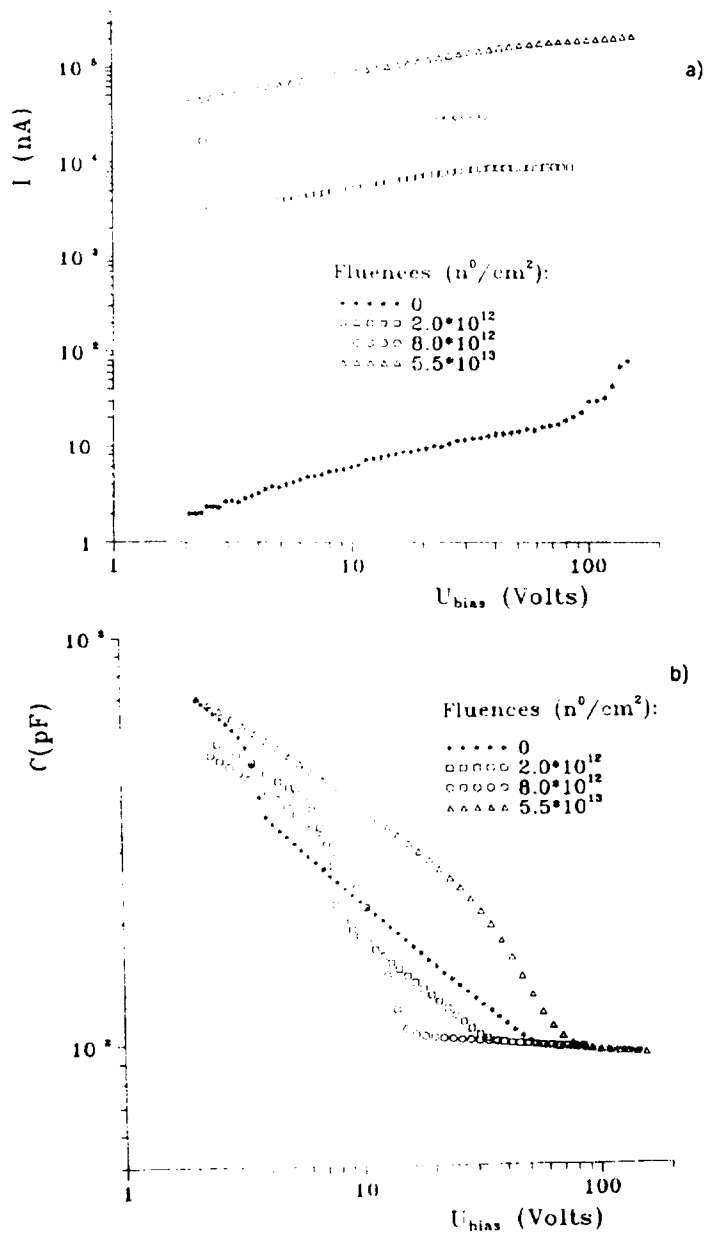


Fig.6. I-V (a) and C-V (b) characteristics of the detector ($20 \times 20 \times 0.4$ mm³ made of Wacker Si and irradiated at different neutron fluences.

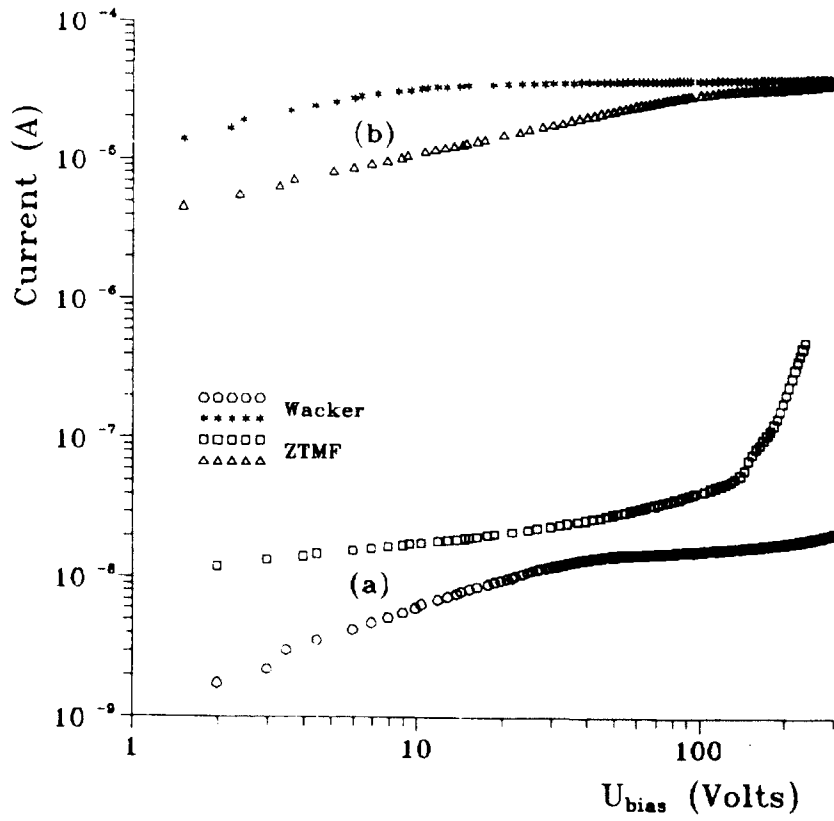


Fig.7. I-V characteristics of the detectors (20x20x0.4) mm³ made of Wacker and ZTMF Si: (a) before and (b) 3 days after neutron irradiation.

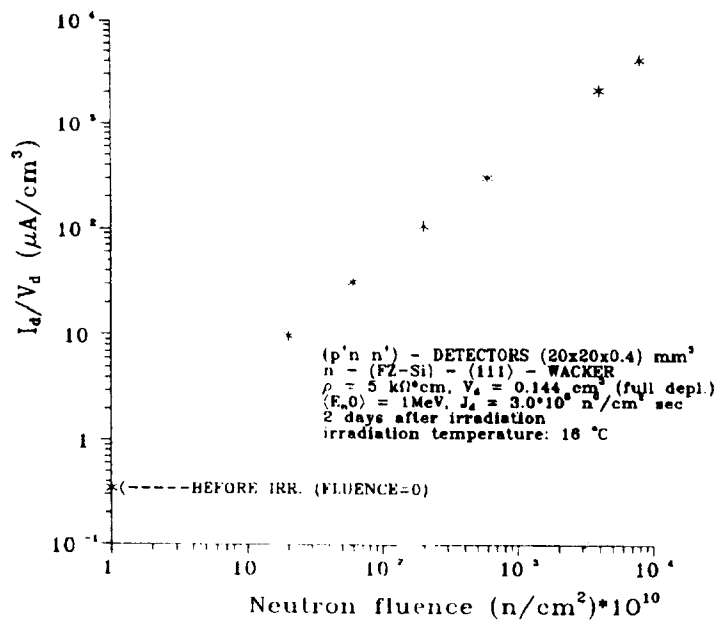


Fig.8. Dependence of the reverse current per volume versus neutron fluence.

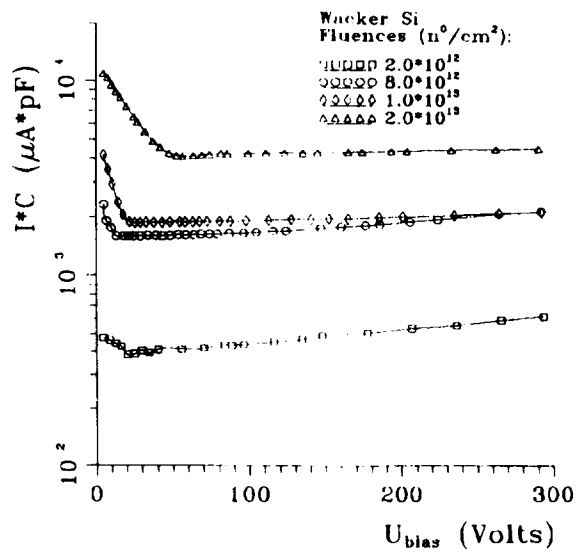


Fig.9. The product $I \cdot C$ versus the reverse bias voltage at different neutron fluences for the detectors (20x20x0.4) mm³

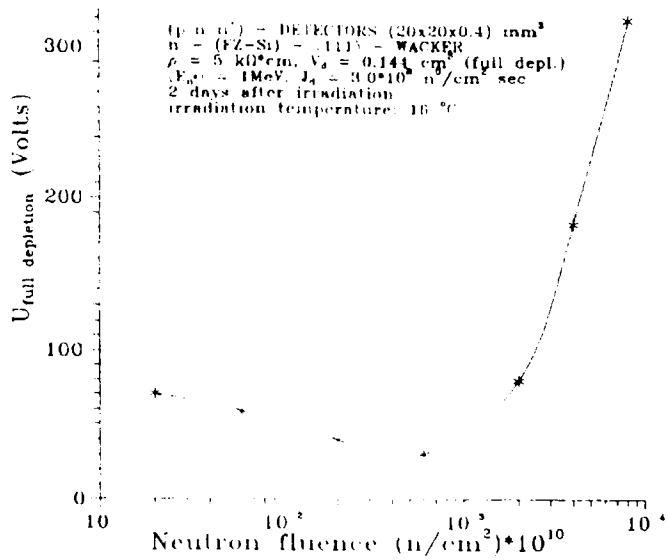


Fig.10. Dependence of the full depletion voltage U_{FD} versus neutron fluence.

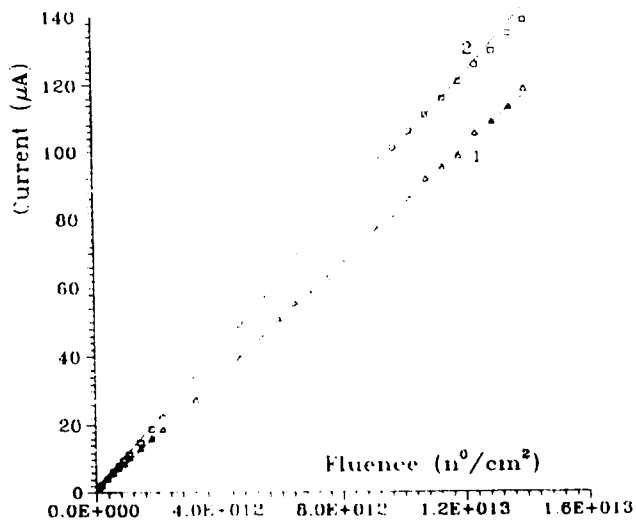


Fig.11. Influence of the reverse bias voltage applied to the detector under neutron irradiation on a reverse current degradation. The current was measured at $U=100$ V.
 (1) - irradiation without reverse bias voltage,
 (2) - irradiation at the reverse bias voltage of 100 V.

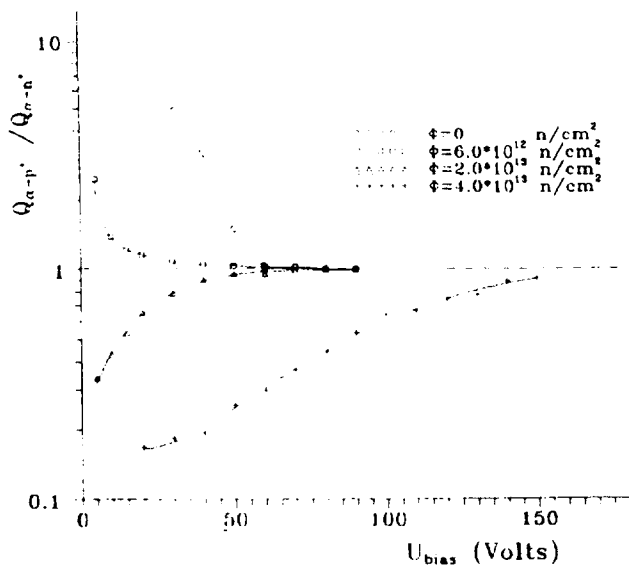


Fig.12. α -particle excitation. Amplitude ratio A_p^+ / A_n^+ at different neutron fluences versus the reverse bias voltage, shaping time — 500 ns.

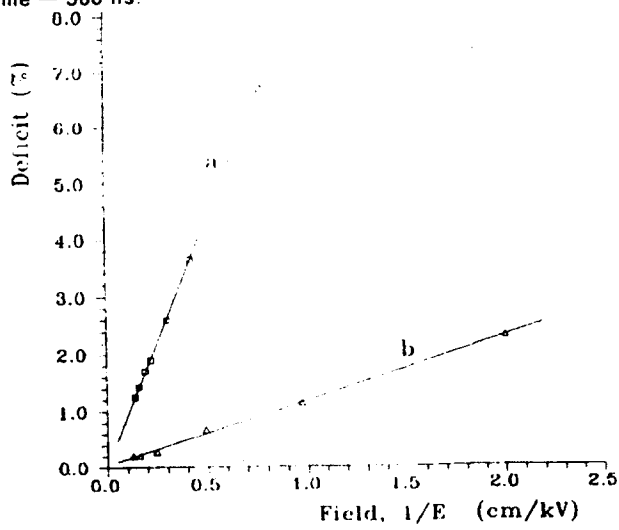


Fig.13. Dependence of the amplitude deficit in the irradiated detector on the electric field. Excitation of non-equilibrium charge carriers by ^{244}Cm α -particles, respectively: (a) — near the n^+ -layer (drift of holes), (b) — near the p^+ -layer (drift of electrons). Fluence: $3.3 \cdot 10^{12} \text{ cm}^{-2}$.

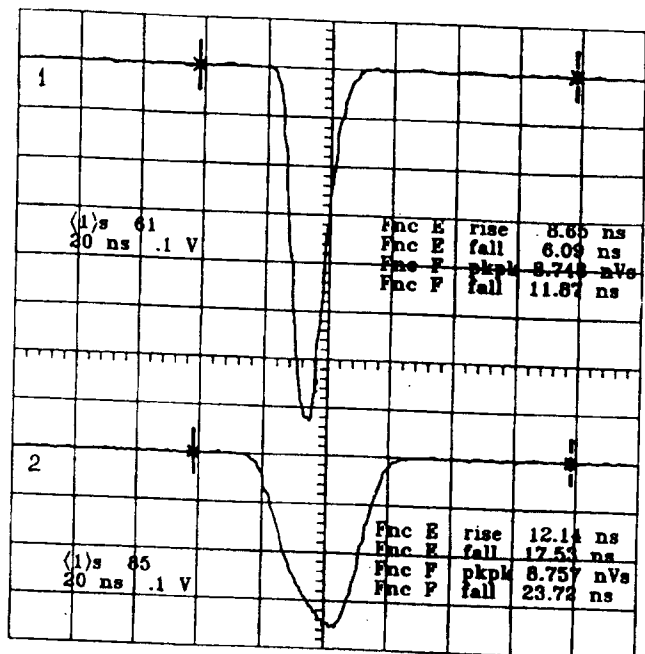


Fig. 14a

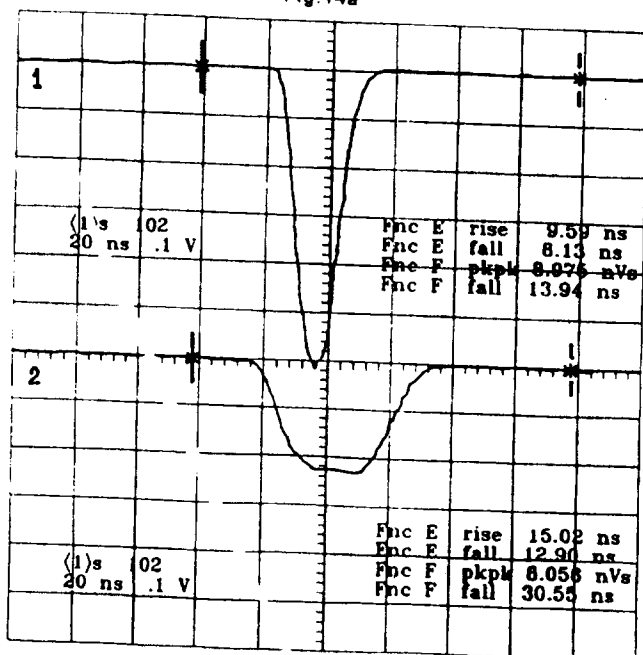


Fig. 14b

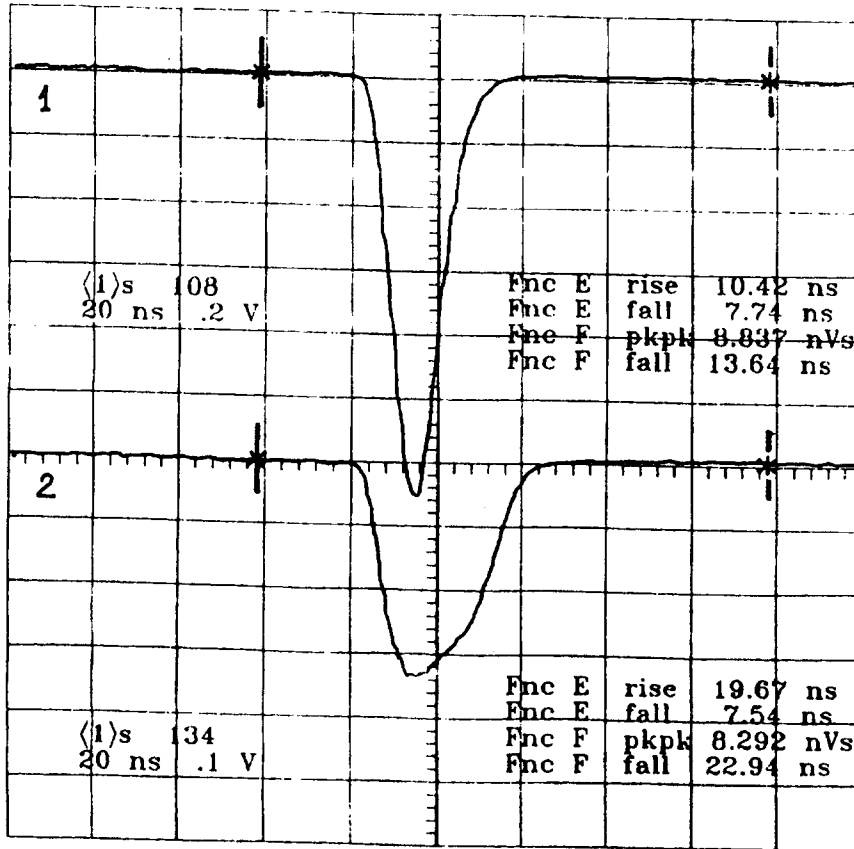


Fig.14c

Fig.14. Current pulse response to the α -particle excitation in the detector: (a) before and (b,c) after neutron irradiation; (1,2) - near the p^+ and n^+ -layer, respectively. Fluence Φ [cm^{-2}]: (b) - $8.0 \cdot 10^{12}$ ($\Phi = \Phi_1$), (c) - $2.0 \cdot 10^{13}$ ($\Phi > \Phi_1$). Reverse bias voltage [V]: (a,c) - 150, (b) - 100.

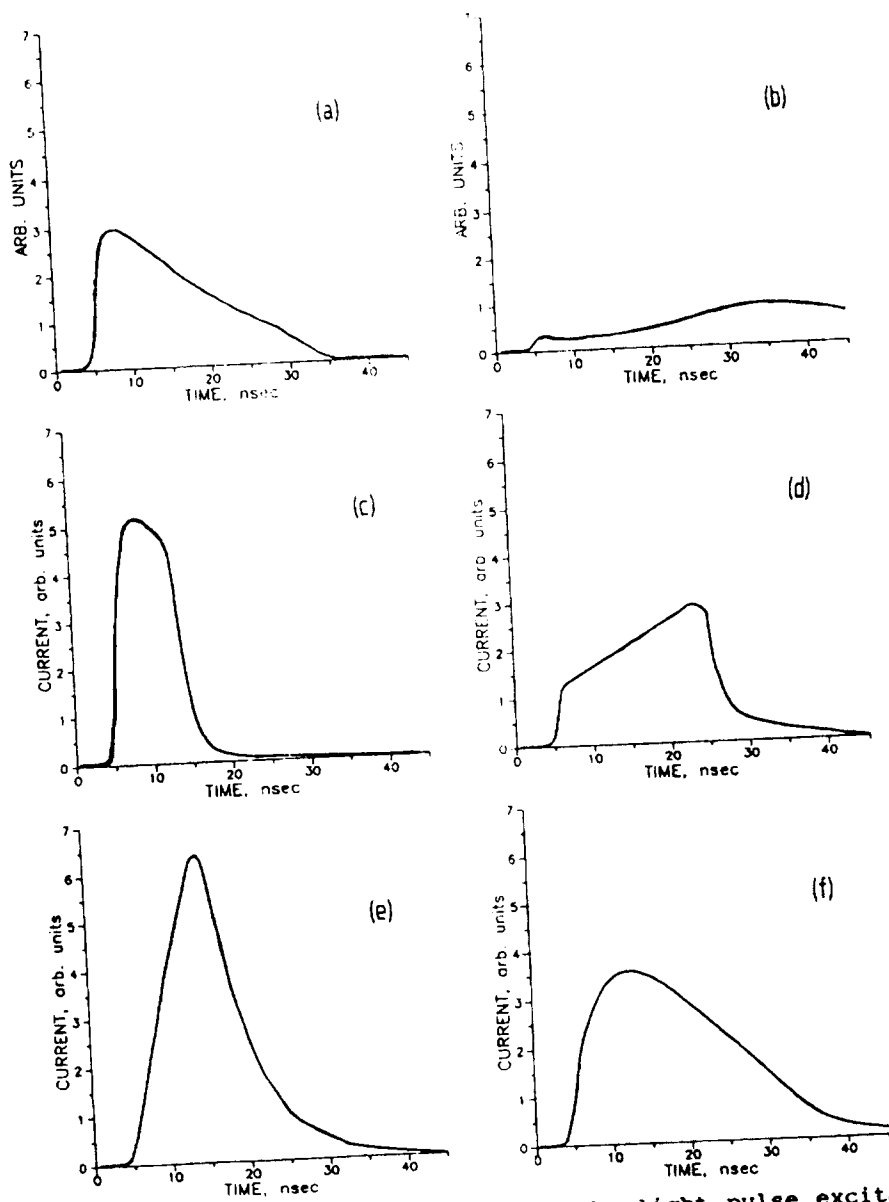


Fig.15. Current pulse response to the light pulse excitation in the non-irradiated (a+d) and irradiated (e,f) detectors. Reverse bias voltage [V]: (a,b) - 70 ($U < U_{FD}$), (c+f) - 1 ($U > U_{FD}$). Fluence ϕ [cm^{-2}]: (e,f) - $3.3 \cdot 10^{13}$ ($\phi > \phi_1$). Light pulse to: (a,c,e) - p^+ -layer, (b,d,f) - n^+ -layer.

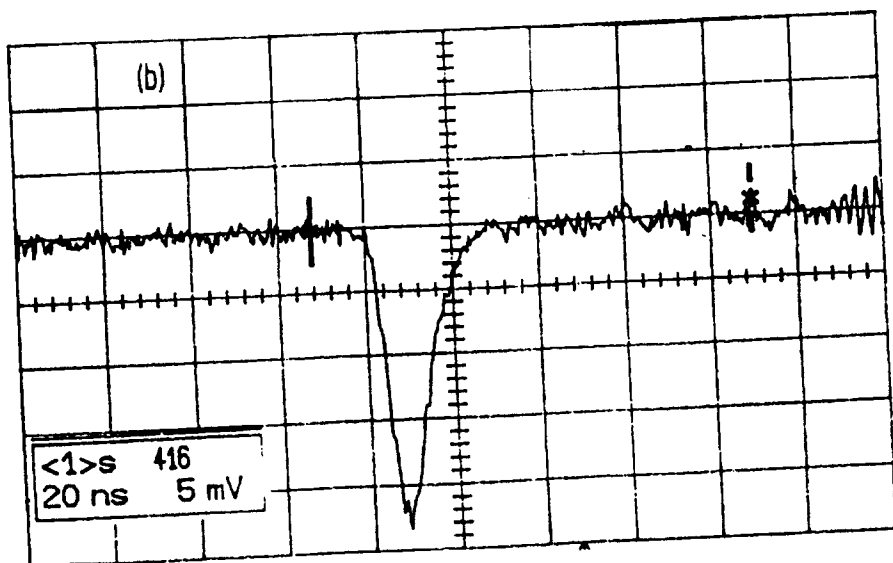
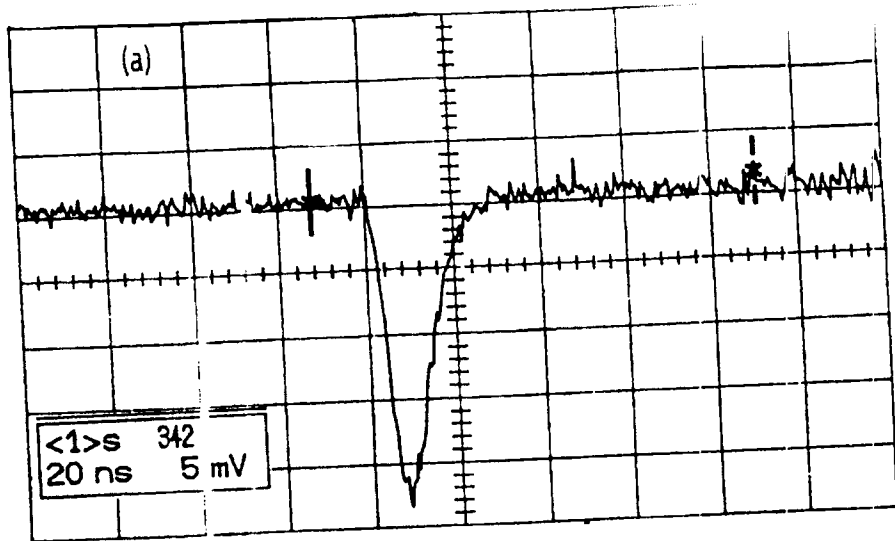


Fig.16. Current pulse response to the m.i.p. excitation in the detector: (a) before and (b) after neutron irradiation. Reverse bias voltage: 250 V, Fluence: $4.0 \times 10^{13} \text{ cm}^{-2}$.

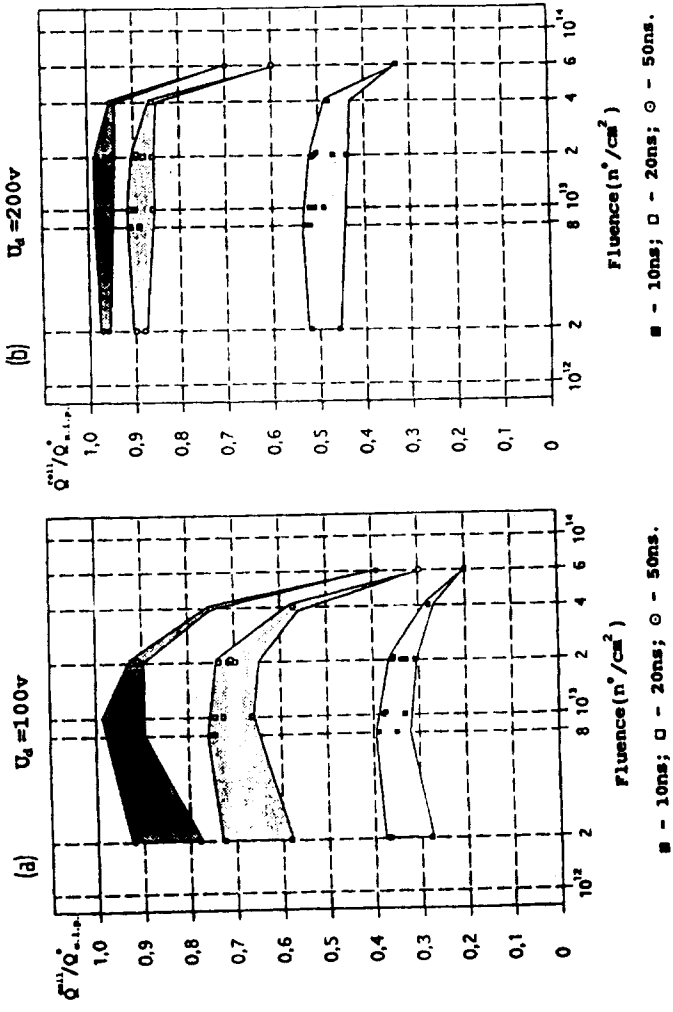


Fig.17. Charge collection efficiency versus neutron fluence calculated from the experimental current pulse curves for the m.i.p. excitation. Reverse bias voltage [V]: (a) - 100, (b) - 200. Integration time [ns]: black squares - 10, squares - 20, circles - 50.

REFERENCES

1. L3P Lepton and Proton Precision Physics. CERN/LHCC 92-5, LHCC/i 3, September 30, 1992.
2. C. Bertrand et al., Silicon Calorimetry for the SSC, Proc. Workshop on Calorimetry for New Supercolliders, eds. R. Donaldson and M.G. Gilchriese, Tuscaloosa, USA.
3. CMS, The Compact Muon Solenoid. Letter of Intent. CERN/LHCC 93-3, LHCC/I1 (1-st October 1992).
4. Addendum to Proposal DRDC/P34, CERN/DRDC92-48, P34 Add.1, January 10, 1993.
5. F. Lemeilleur et al., Electrical Properties and Charge Collection Efficiency for Neutron Irradiated p-type and n-type Silicon Detectors, CERN/ECP 92-12.
6. A. Quaranta, G. Casadei, M. Martini, G. Ottaviani, G. Zapparini, Nucl. Instr. and Meth., 35 (1965) 93.
7. E.M. Verbitskaya, V.K. Eremin, N.B. Strokan, J. von Borany and B. Schmidt, Nucl. Instr. and Meth., A281 (1989) 167.
8. V.M. Nazarov, V.F. Peresedov, V.P. Sysoev, JINR Preprint 6-85, Dubna, 1985, 42 p.
9. A.I. Voytov, V.M. Nazarov, V.A. Poyarkov, V.F. Peresedov, JINR Preprint R3-86-155, Dubna, 1982.
10. B.R. Gossick, J. Appl. Phys., 30 (1959) 1214.
11. M. Bruzzi, A. Baldini, E. Borchi and I. Lukianov, Nucl. Instr. and Meth., A326 (1993) 344.
12. M.T. Asom, J.L. Benton, R. Sauer and L.C. Kimerling, Appl. Phys. Lett., 51 (1987), #4, 256.
13. L.W. Song, B.W. Benson and G.D. Watkins, Appl. Phys. Lett., 51 (1987), #15, 1155.
14. E. Borchi et al., Nucl. Instr. and Meth., A279 (1989) 277.
15. P.V. Kuchinsky and V.M. Lomako, Solid State Electron., 26 (1986) 1041.
16. E.M. Verbitskaya, V.K. Eremin, A.V. Ivanov, N.B. Strokan, Semiconductors 27, 2, (1993), 115.
17. V.V. Voronkov et. al., Fiz. Techn. Poluprov., 16 (1982) 1752.

18. A.Chantre and L.S.Kimerling, Appl. Phys. Lett., 48, 15, (1986), 1000.
20. E.Verbitskaya et al., Relaxation of Radiation Damages in Silicon Planar Detectors, presented at the 1-st Intern. Conf. on Large Scale Application of Semicond. Detect. and Rad. Hardness, Florence, July 7-9, 1993.
21. E.M.Verbitskaya, V.K.Eremin, A.M.Ivanov, N.B.Strokan, Semiconductors, 27, 7, (1993) 1113.
22. E.Fretwurst et al., Reverse Annealing of the Effective Concentration and Long Term Operational Scenario for Silicon Detectors in Future Collider Experiments, presented at Int. Symp. on Application of Sem. Track. Det., Japan, May 1993.
23. H.W.Kraner and Z.Li, Nucl. Instr. and Meth., A279 (1989) 266.
24. E.Borchi et al., Nucl. Instr. and Meth., A301 (1991) 215.
25. R.Wunstorff et al., Nucl. Instr. and Meth., A315 (1992) 149.
26. Z.Li and H.W.Kraner, BNL report #36210, Sept. (1991).
27. H.W.Kraner, Z.Li and E.Fretwurst, Nucl. Instr. and Meth., A326 (1993) 350.
28. Z.Li, V.Eremin, N.Strokan and E.Verbitskaya. IEEE Trans., Nucl. Sci., NS-40 (1993) 3367.
29. A.Quaranta, A.Taroni and G.Zanarini, IEEE Trans. Nucl.Sci., NS- 15 (1968), 373.
30. A.Gillespie, Signal Noise and Resolution in Nuclear Counter Amplifiers, Pergamon Press, New-York, 1953.

Received by Publishing Department
on March 3, 1995.

Принимается подписка на препринты, сообщения Объединенного института ядерных исследований и «Краткие сообщения ОИЯИ».

Установлена следующая стоимость подписки на 12 месяцев на издания ОИЯИ, включая пересылку, по отдельным тематическим категориям:

Индекс	Тематика	Цена подписки на год
1.	Экспериментальная физика высоких энергий	22600 р.
2.	Теоретическая физика высоких энергий	59200 р.
3.	Экспериментальная нейтронная физика	7800 р.
4.	Теоретическая физика низких энергий	23400 р.
5.	Математика	14800 р.
6.	Ядерная спектроскопия и радиохимия	12000 р.
7.	Физика тяжелых ионов	2200 р.
8.	Криогеника	1400 р.
9.	Ускорители	12200 р.
10.	Автоматизация обработки экспериментальных данных	12200 р.
11.	Вычислительная математика и техника	14300 р.
12.	Химия	1200 р.
13.	Техника физического эксперимента	21300 р.
14.	Исследования твердых тел и жидкостей ядерными методами	7200 р.
15.	Экспериментальная физика ядерных реакций при низких энергиях	2600 р.
16.	Дозиметрия и физика защиты	2200 р.
17.	Теория конденсированного состояния	12200 р.
18.	Использование результатов и методов фундаментальных физических исследований в смежных областях науки и техники	1800 р.
19.	Биофизика	1800 р.
	«Краткие сообщения ОИЯИ» (5—6 выпусков)	15000 р.

Подписка может быть оформлена с любого месяца года.

Организациям и лицам, заинтересованным в получении изданий ОИЯИ, следует перевести (или отправить по почте) необходимую сумму на расчетный счет 000608905 Дубненского филиала ММКБ, г.Дубна Московской области, п/инд. 141980 МФО 211844, указав: «За подписку на издания ОИЯИ».

Во избежание недоразумений необходимо уведомить издательский отдел о произведенной оплате и вернуть «Карточку подписчика», отметив в ней номера и названия тематических категорий, на которые оформляется подписка, по адресу:

141980 г. Дубна Московской обл.
ул. Жолио Кюри, 6
ОИЯИ, издательский отдел

**Радиационная стойкость кремниевых детекторов
для экспериментов на коллайдерах**

Исследованы планарные кремниевые детекторы до и после облучения быстрыми нейтронами ($\langle E_{n,0} \rangle = 1,35$ МэВ) при комнатной температуре. Максимальный флюенс нейтронов составил $8 \cdot 10^{13} \text{ см}^{-2}$. Детекторы изготавливались из высокоомного ($1 + 10 \text{ кОм} \cdot \text{см}$) зонно-очищенного (FZ) кремния p-типа с ориентацией $\langle 111 \rangle$. Использовался кремний, полученный от двух различных производителей: WACKER CHEMITRONIC и Запорожского титано-магниевого комбината (ЗТМК). Исследовано влияние облучения быстрыми нейтронами на основные параметры исходного кремния, не прошедшего высокотемпературных технологических операций.

Работа выполнена в Лаборатории сверхвысоких энергий ОИЯИ.

Препринт Объединенного института ядерных исследований. Дубна, 1995

Golutvin I.A. et al.

E14-95-97

Radiation Hardness of Silicon Detectors for Collider Experiments

The silicon planar detectors before and after fast neutron irradiation ($\langle E_{n,0} \rangle = 1.35$ MeV) at room temperature have been investigated. Maximal neutron fluence has been $8 \cdot 10^{13} \text{ cm}^{-2}$. The detectors have been manufactured of the high resistivity ($1 + 10 \text{ кOhm} \cdot \text{cm}$) n-type float-zone silicon (FZ-Si) with the $\langle 111 \rangle$ orientation supplied by two different producers: WACKER CHEMITRONIC and Zaporozhje Titanium-Magnesium Factory (ZTMF). The influence of fast neutron irradiation on the main parameters of the starting silicon before the technological high temperature treatment has been investigated as well.

The investigation has been performed at the Laboratory of Particle Physics, JINR.

Preprint of the Joint Institute for Nuclear Research. Dubna, 1995

Макет Т.Е.Попеко

**Подписано в печать 19.05.95
Формат 60×90/16. Офсетная печать. Уч.-изд.листов 3,12
Тираж 340. Заказ 48208. Цена 1872 р.**

**Издательский отдел Объединенного института ядерных исследований
Дубна Московской области**